

A numerical study of wave dispersion curves in cylindrical rods with circular cross-section

G. Valsamos^{a,*}, F. Casadei^a, G. Solomos^a

^a Joint Research Centre, European Laboratory for Structural Assessment (IPSC/ELSA), I-21027 Ispra (VA), Italy

Received 7 February 2013; received in revised form 2 May 2013

Abstract

This work presents a finite element approach for modeling longitudinal wave propagation in thick cylindrical rods with circular cross-section. The formulation is based on simple time domain response of the structure to a properly chosen excitation, and is calculated with an explicit finite element solver. The proposed post-treatment procedure identifies the wavenumber for each mode of wave propagation at the desired frequency. The procedure is implemented and integrated in an efficient way in the explicit finite element code Europlexus. The numerical results are compared to the analytical ones obtained from the solution of the Pochhammer — Chree equation, which provides the dispersion curves for wavetrains in solid cylinders of infinite length.

© 2013 University of West Bohemia. All rights reserved.

Keywords: dispersion curves, Pochhammer-Chree equation, wave propagation in rods, explicit finite element analysis, mode identification

1. Introduction

The phenomenon of dispersion is the reason why waves with different wavelengths travel at different speeds in the same material. This phenomenon appears in a cylindrical rod when the radius of the rod is comparable to the wavelength of the wave propagated in it. The magnitude of the effect depends also on the Poisson's ratio value of the material. Dispersion needs to be taken into account in several cases, for example, in the propagation of ultrasonic signals in solid waveguides, or in the high strain-rate testing with a Hopkinson bar apparatus [9, 15]. The strain pulses travelling in the incident and transmitter bars undergo this type of dispersion, and results of better quality are obtained if a correction, based on dispersion theory is performed.

The exact formulation of the wave equation in an infinite long cylindrical bar of circular cross-section was first given by Pochhammer in 1876 [16] and independently by Chree in 1889 [5]. Pochhammer transformed the three-dimensional equation of motion of a solid circular rod into cylindrical coordinates, and by applying the boundary conditions for traction-free surfaces, the frequency equation was derived. This equation relates the propagation velocity C_p (phase velocity) of the *longitudinal waves* to the wavelength Λ for each mode. However, due to its complexity, numerical solutions of this frequency equation were only obtained much later [2]. Wave propagation in rods and the Pochhammer-Chree equation have been exhaustively treated analytically, e.g. by Graff [11], Kolsky [13] and Love [14].

In the present work a study has been conducted on the numerical identification of the longitudinal vibration modes, and on the capability of the Europlexus code [8] to capture wave dispersion in cylindrical rods with circular cross-section. Europlexus is a fast transient dynamics

*Corresponding author. Tel.: +390 332 789 004, e-mail: georgios.valsamos@jrc.ec.europa.eu.

explicit Finite Element code suitable for simulating wave propagation and transient dynamics phenomena in continuous media.

A new tool has been developed for the calculation of the dispersion curves from numerical simulations, where two different methodologies have been implemented. As in [16], in both cases dynamic excitation in the axial direction is applied at one end of a semi-infinite rod, but a more efficient excitation scheme has been introduced in this study. The identification of the contributing modes is based on Fourier transform techniques of the calculated structural response both in the time and in the space domains.

The dispersion curves resulting from the numerical simulations are compared with the analytical ones obtained by solving the corresponding Pochhammer-Chree equation. The performance of the methodologies for various models, with respect to the type of finite elements employed (e.g. linear, parabolic etc.) and to the fineness of the mesh, is discussed and assessed. An investigation of the influence of Poisson's ratio on the dispersion curves has also been carried out.

2. Pochhammer-Chree analytical equation for cylindrical geometries

The Pochhammer-Chree frequency equation is derived along the formulation of the equation of motion for the propagation of a sinusoidal wavetrain of frequency ω in an infinite long bar of circular cross-section, when the equation of motion is transformed into cylindrical coordinates and the boundary conditions for traction-free surfaces are applied. This frequency equation, relating the propagation velocity C_p (phase velocity) of the *longitudinal waves* to the wavelength, may be solved for any frequency ω . A comprehensive study of the Pochhammer-Chree solution is given by Redwood [19], who for conciseness rewrites the equation in the form:

$$k^2 q \frac{J_0(qa)}{J_1(qa)} + \left[-\frac{1}{2} \left(\frac{\omega}{C_t} \right)^2 \right] \frac{1}{a} + \left[\frac{1}{2} \left(\frac{\omega}{C_t} \right)^2 - k^2 \right] \frac{J_0(pa)}{J_1(pa)p} = 0, \quad (1)$$

where:

$$p = \sqrt{(\omega/C_l)^2 - k^2}, \quad q = \sqrt{(\omega/C_t)^2 - k^2}, \quad C_l = \sqrt{(\lambda + 2\mu)/\rho}, \quad C_t = \sqrt{\mu/\rho}. \quad (2)$$

In these expressions a is the radius of the rod, C_l and C_t are, respectively, the velocities of dilatational and shear waves (transverse waves) in an unbounded medium, λ and μ are Lamé's constants, ν is Poisson's ratio, E is Young's modulus and ρ is the material density. Finally, $J_0(x)$ and $J_1(x)$ are the Bessel functions [1] of the first kind of order zero and one, respectively.

For a propagating wave of angular frequency ω , Eq. (1) becomes a nonlinear algebraic equation with only one unknown, the wavenumber k . Such an algebraic equation has multiple (real) roots k_i , each one corresponding to the wavenumber of the i^{th} propagating mode. The largest root corresponds to the first mode, the second largest root corresponds to the second mode, and so on. Several efficient iterative methods to solve such a nonlinear algebraic equation exist, e.g. Newton-Raphson procedures [7].

By calculating the wavenumber for all the frequencies of interest relative to a mode, the dispersion curve for that mode can be fully determined. Fig. 1 shows the dispersion curves of the first four modes for a material with Poisson's ratio $\nu = 0.3$. The ordinates have been normalized by dividing the phase velocity C_p by the fundamental velocity $C_0 = (E/\rho)^{1/2}$.

From the curve of the first mode it is evident that for low values of a/Λ the phase velocity is almost identical to C_0 . It is also easily noted that the phase velocity decreases with decreasing

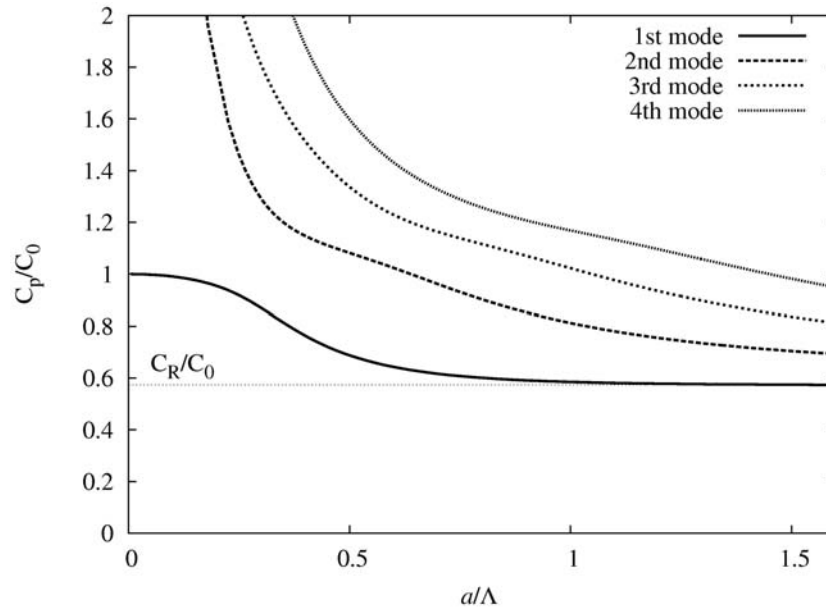


Fig. 1. Dispersion curves for the first 4 modes for a material with Poisson's ratio $\nu = 0.3$

wavelength, which means that high-frequency waves travel slower than lower-frequency waves. As a/Λ increases, the value of C_p tends asymptotically to C_R , where C_R is the velocity of the Rayleigh surface waves of the medium [17]. For the second and higher modes the so-called cut-off frequencies are present, where the phase velocity tends to infinity. In this case, if $C_p \rightarrow \infty$, $k \rightarrow 0$, from Eq. (2) $p = \omega/C_l$ and $q = \omega/C_t$, and finally it can be shown [17] that the cut-off frequencies of the modes can be determined by the equations:

$$\left(\frac{\omega}{C_l}a\right) J_0\left(\frac{\omega}{C_l}a\right) / J_1\left(\frac{\omega}{C_l}a\right) = 2\left(\frac{C_t}{C_l}\right)^2 \quad \text{or} \quad J_1\left(\frac{\omega}{C_t}a\right) = 0. \quad (3)$$

The cutoff frequency of a particular mode is the lowest frequency at which the mode can be observed. As seen in Fig. 1, at larger frequencies the phase velocities of the higher modes also decrease rapidly and then reach asymptotically constant values.

3. Numerical approach

3.1. Time domain response

An accurate prediction of the dynamic response of complex mechanical systems can be achieved by the finite element method [12]. In particular, for fast transient dynamic phenomena, such as wave propagation, impacts, blasts etc [3], the explicit finite element is overall more efficient. The wave dispersion effect, which is the subject of the current study, is typical of wave propagation in structures. By assuming a linear, small-strain formulation the problem can be described by the following system of differential equations:

$$\mathbf{M}\ddot{\mathbf{u}} + \mathbf{K}\mathbf{u} = \mathbf{f}^{\text{ext}}, \quad (4)$$

where \mathbf{M} is the mass matrix, \mathbf{K} is the stiffness matrix, \mathbf{f}^{ext} the vector of the external applied loads, \mathbf{u} and $\ddot{\mathbf{u}}$ are the displacement and the acceleration vector of the nodes of the structural model respectively. Equation (4) can be also expressed more generally as:

$$\mathbf{M}\ddot{\mathbf{u}} = \mathbf{f}^{\text{ext}} \boldsymbol{\sigma} - \mathbf{f}^{\text{int}} = \mathbf{f}^{\text{ext}} - \sum_e \int_{V_e} \mathbf{B}^T dV, \quad (5)$$

where σ is the stress induced in the structure, \mathbf{B} is the matrix of shape function derivatives and V^e represents the element (e) volume. The set of equations (5) is rendered fully explicit (decoupled) through diagonalization, via a suitable lumping process of the matrix \mathbf{M} . The accelerations are directly obtained, without any need for system solutions.

The time integration of Eq. (5) is achieved via a central difference scheme, which is usually written as:

$$\begin{aligned}\dot{\mathbf{u}}^{n+1} &= \dot{\mathbf{u}}^n + \frac{\Delta t}{2} (\ddot{\mathbf{u}}^n + \ddot{\mathbf{u}}^{n+1}), \\ \mathbf{u}^{n+1} &= \mathbf{u}^n + \Delta t \left(\dot{\mathbf{u}}^n + \frac{\Delta t}{2} \ddot{\mathbf{u}}^n \right).\end{aligned}\quad (6)$$

The upper index n denotes a quantity at time t^n and $n + 1$ denotes a quantity at time $t^{n+1} = t^n + \Delta t$, Δt being the time interval used in the discretization process. The steps of the procedure are as follows. Assume that a complete solution, i.e. all discretized quantities (displacements \mathbf{u} , velocities $\dot{\mathbf{u}}$, accelerations $\ddot{\mathbf{u}}$, stresses σ and related variables) are known at time t^n . First, an intermediate (half-step) velocity is introduced:

$$\mathbf{v}^{n+1/2} = \dot{\mathbf{u}}^n + \frac{\Delta t}{2} \ddot{\mathbf{u}}^n, \quad (7)$$

which is denoted as \mathbf{v} in order to distinguish it from $\dot{\mathbf{u}}$. This is the constant velocity that would transform configuration n into configuration $n + 1$ over a time interval Δt in the discretization process. From the second of Eqs. (6), the new displacements are given by:

$$\mathbf{u}^{n+1} = \mathbf{u}^n + \Delta t \mathbf{v}^{n+1/2}. \quad (8)$$

On this new configuration, the stress σ^{n+1} can now be evaluated by application of the constitutive relations. Then, the new field of accelerations $\ddot{\mathbf{u}}^{n+1}$ can be directly computed via the discretized equilibrium equation (5) and finally the new velocities are obtained from the first of Eqs. (6).

It is noted that this time integration scheme is explicit in that all the quantities in the right-hand side terms are known when the equations are applied, thus no system solver is needed [4]. For the explicit integration scheme the Courant condition for the time step must be satisfied, which states that the wavefront cannot travel farther than one element in one time step [20]. This condition, which ensures stability, leads to very small time steps but, in the case of fast transient dynamics, this is not really a limitation because small steps would be needed anyway to achieve the desired accuracy.

3.2. Structural model

The basic structure used for this investigation is a cylindrical rod with circular cross-section, of radius $a = 0.00635$ m and length $L = 0.508$ m. The chosen ratio $L/a = 80$ is sufficient to simulate a semi-infinite cylindrical rod. The material properties of the rod are: Young's modulus $E = 2.068 \times 10^{11}$ Pa, density $\rho = 7822.8$ kg/m³ and Poisson's ratio $\nu = 0.3$. The axial load is applied at one end of the cylindrical rod, and the final time for the calculation is taken to be $T_{end} = 9 \times 10^{-5}$ s, just short for the wavefront to arrive at the free end of the rod. A 2D axisymmetric numerical model is employed in order to decrease the cost of the numerical calculation with respect to a full 3D model. The y -axis of the mesh coincides with the axis of symmetry of the rod and all nodes along this axis are blocked in the radial direction. The x -axis of the mesh coincides with the radius of the rod. Only the portion of the rod's longitudinal cross section at $x \geq 0$ is included in the axisymmetric numerical model. The formulation assumes that only 1 radian of the cylinder is modeled in the azimuthal direction (θ) and therefore a factor

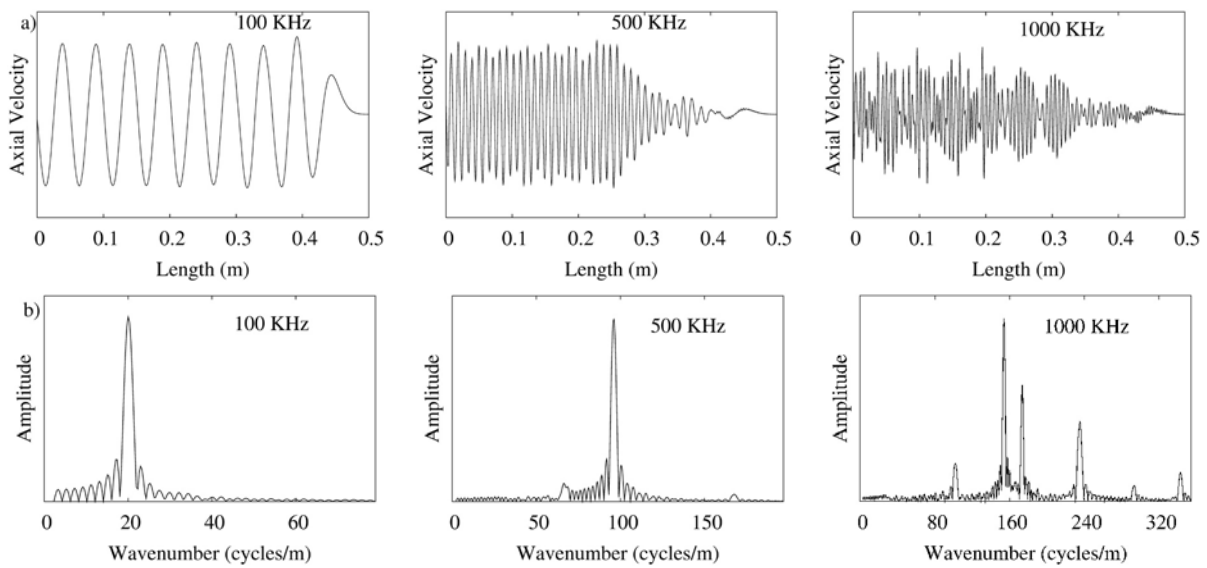


Fig. 2. a) Spatial distribution of axial velocity over the nodes at distance $3/4$ of the radius from the cylinder axis at time $t = T_{end}$, b) the corresponding wavenumber spectra

2π should be considered when comparing extensive results (e.g. total mass, total axial force etc.) with those that would be obtained in a formulation modeling the entire rod.

The finite element model used for the main set of results has 32 000 4-node quadrilateral elements (20 elements in the radial direction and 1600 elements in the axial direction). This model is selected because it ensures the minimum number of elements per wavelength. After many simulations it has been observed that a model with at least 5 elements per wavelength gives sufficient accuracy in the results. This limit is based on the smallest wavelength or the highest wavenumber. Once the time response of the structure has been obtained, a post treatment procedure of the numerical results is applied in order to determine the wave dispersion curves. For all transforms the Fast Fourier Transformation scheme [6] is used.

3.3. Single harmonic excitation

The first methodology to calculate the desired curves uses an excitation load applied at the one extremity of the rod in the direction parallel to its axis, which is a harmonic time-dependent pressure $P(t)$ of the form:

$$P(t) = P_o \sin(2\pi f_i t). \quad (9)$$

This type of load forces the particles of the structure to eventually vibrate in frequency f_i , so that the numerical results of the response will contain information only for that specific frequency. The disturbance is transmitted along the cylindrical rod and the analysis of the time history of the response produces the desired results. As noted above, the final time of the calculation must be less than the time needed for the wavefront to reach the other extremity of the bar. This limitation is due to the fact that the results should be clear of any reflections.

Since all data from the time integration up to the final time step are available, it is possible to reconstruct the motion over the space domain. This reconstruction of the space distribution of the response is done for points (nodes) lying in selected lines parallel to the axis of the cylindrical rod. Fig. 2a depicts the space distributions of the axial velocity at the final time step ($t = T_{end}$), along a line parallel to the axis of the cylinder at $3/4$ of its radius, for three different excitation frequencies. As it can be observed from this figure, the wavefront has not yet reached

the extremity of the bar opposite to the loaded end, and this guarantees that no contaminating reflections at the free end have occurred yet.

In this study, the selected response parameter is the axial velocity, which is considered to be the most representative one, although others such as the displacement or stresses could have been chosen, too. Clearly the space distribution can be generated along more than one lines, at different distances from the axis of symmetry, in order to avoid omitting information from a certain mode whose contribution at a specific distance from the center may be very small or even zero (nodal point). In this manner it is assured that all modes of the wave propagation can be determined in the next step of the post-treatment procedure.

The space distribution of the chosen response parameter can be used in order to determine the wavenumber spectrum for the frequency f_i under consideration. The transition from the space distribution to the wavenumber spectrum is achieved through a discrete Fourier transform according to the following equations:

$$\begin{aligned} V'[k] &= \sum_{z=0}^{M-1} V[z] e^{-i(2\pi/M)zk}, & k = 0, 1, \dots, M-1, \\ V[z] &= \frac{1}{M} \sum_{k=0}^{M-1} V'[k] e^{i(2\pi/M)zk}, & z = 0, 1, \dots, M-1. \end{aligned} \quad (10)$$

The pair of equations (10) expresses the direct and the inverse transformation, where $V[z] = V(z_j)$, $j = 0, \dots, M-1$ is the space distribution of the axial velocity and $V'[k] = V'(k_j)$, $j = 0, \dots, M-1$ is its computed transform in the wavenumber domain; M is the number of transformed points (equal to the number of nodes along the selected line plus the zero padding points, as explained below) and $i = \sqrt{-1}$.

The wavenumber spectrum (amplitude of $V'[k]$) for each line can next be readily generated, and the sought information can be extracted since the peaks can be identified through a search algorithm: each peak on this spectrum corresponds to the wavenumber value of a *longitudinal* mode for the frequency $f_i = \omega_i/2\pi$ under consideration. The peak with the largest wavenumber value refers to the first mode of wave propagation (this is evident for all frequencies f_i since there is no cut-off frequency for the first mode). The peak with the second-largest wavenumber value refers to the second mode, and so on. Fig. 2b illustrates the wavenumber spectrum for three different frequencies. When the excitation frequency is $f_i = 100$ kHz only one peak is observed, since for that frequency only the first mode can be activated. For the other two frequencies more peaks can be observed, which correspond to higher *longitudinal* modes. Fig. 3a shows the identified peaks for a frequency $f_i = 780$ kHz. As already mentioned, it is necessary to use data from more than one lines parallel to the axis of the rod, as some of the modes might be difficult to be identified from the space distribution data set at a certain location. For the current study it has been found that four such “processed” lines should suffice, namely those at distances from the rod axis of symmetry equal to $1/4, 2/4, 3/4$ and $4/4$ radii.

Thus for a certain frequency f_i , one or more wavenumber values k_{ij} are determined depending on whether a particular mode j exists or not for that frequency ($j = 1, 2, 3, \dots$), and one point for each mode dispersion curve is calculated, with its (X, Y) coordinates being expressed as:

$$\text{for each } f_i : \quad X_j = \frac{ak_{ij}}{2\pi} = \frac{a}{\Lambda_j}, \quad Y_j = \frac{\omega_i}{k_{ij}C_0} = \frac{C_{p,j}}{C_0}. \quad (11)$$

Clearly Λ_j is the wavelength for mode j and $C_{p,j}$ the corresponding phase velocity. It is recalled that for a propagating harmonic wave of frequency $f = \omega/2\pi$ and wavenumber k , these quantities are connected by the relationships: $C_p = \omega/k$ and $\Lambda = 2\pi/k$.

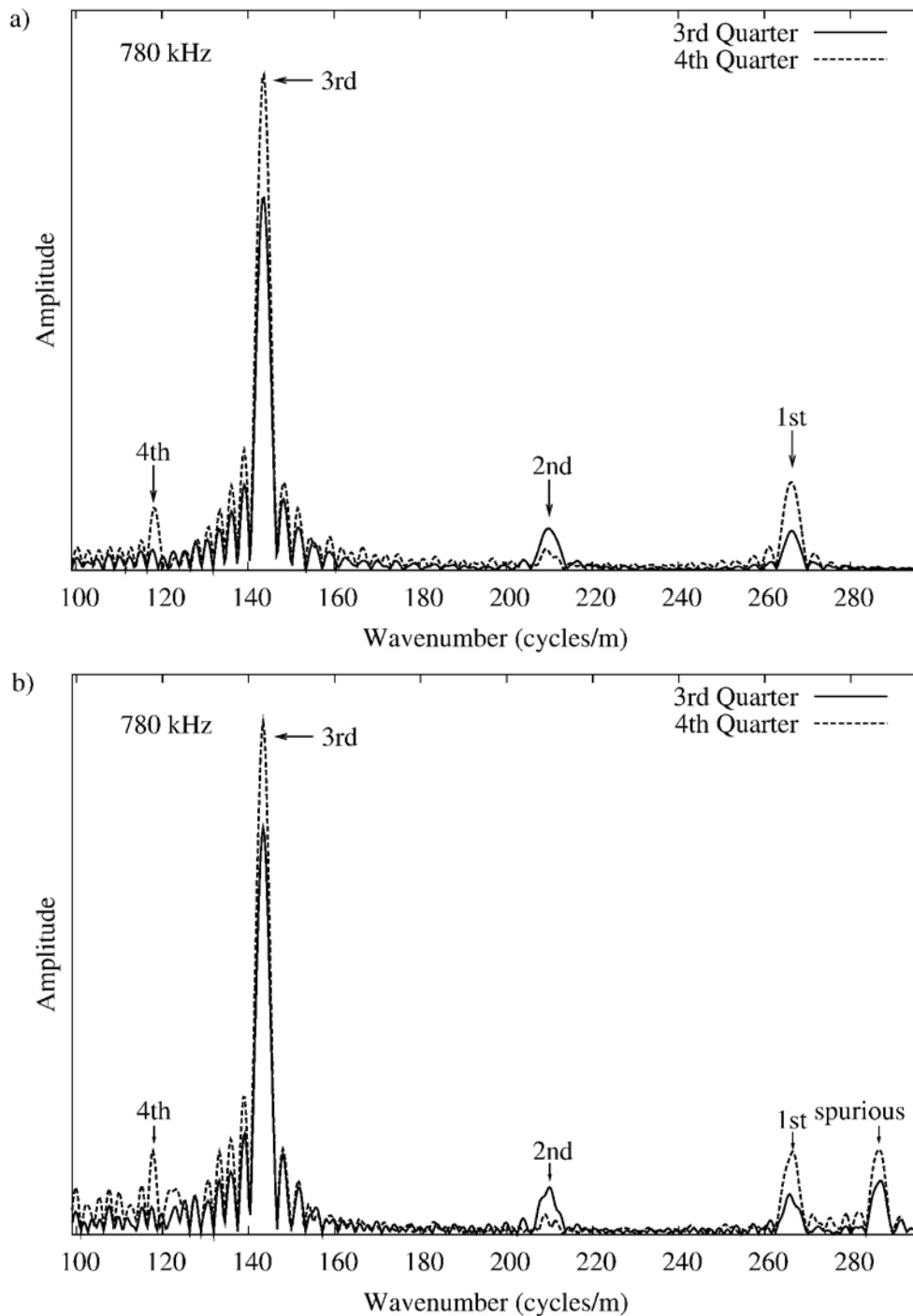


Fig. 3. Modes identification in the wavenumber spectrum at 780 kHz a) with a harmonic load excitation, b) with a step function load

The set of points obtained after one simulation corresponds to one frequency f_i and this implies that, in order to have the complete set of points to construct the curves, the procedure must be repeated many times (i.e., for a wide range of frequencies). The number of simulations with this methodology is equal to the number of points needed per dispersion curve. From this fact it is obvious that, although the methodology is accurate and straightforward, the time required for the complete calculation of a smooth enough curve makes this methodology inefficient. Therefore another methodology has been developed, as described in the next section.

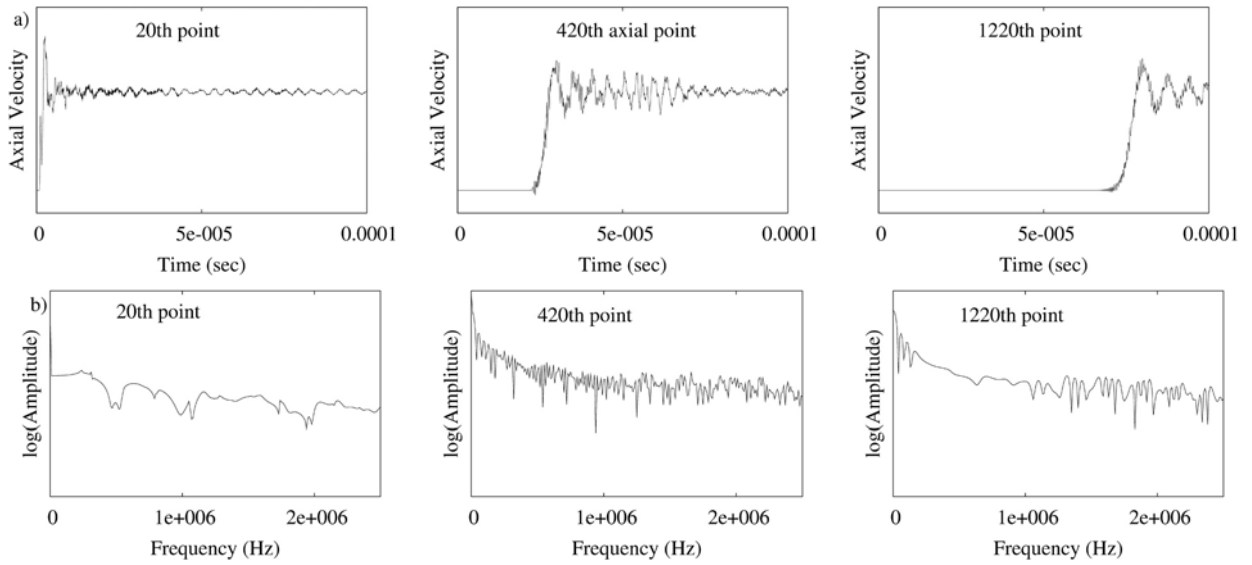


Fig. 4. a) Time histories for three points along a straight line, b) the corresponding frequency spectra

3.4. Step function excitation

A principal objective of the second methodology is to reduce the number of numerical simulations necessary to construct the dispersion curves. This could be achieved only if the response of a single simulation contains information for all the frequencies under consideration. To this end, a broad-band excitation should be used, for example, a step-function load. Such a load can trigger all the frequencies of interest in the structure and the corresponding numerical results of the response will contain information for all those frequencies. The time response of the structure under a step-pressure excitation contains information for all the frequencies, but it is difficult to determine which wavenumber belongs to a particular frequency. For that reason, it is necessary to apply an extra procedural step to separate the contribution of each frequency.

The target of this extra step is to reconstruct the space distribution along a line parallel to the axis of the cylinder, for each frequency of excitation. In order to achieve this, first the time response for all the points along the desired line must be extracted from the numerical results. Fig. 4a depicts the time histories for three points along a line parallel to the axis of the cylinder. The first sub-picture refers to a node near the loaded end of the cylinder. Clearly this node is set to motion almost from the very beginning, as the pressure wave arrives there very early. In the other sub-pictures, referring to nodes at locations corresponding to the 1st, and 3rd quarter of the length of the cylinder, there is an initial quiescent period, since the pressure wave has not yet arrived at these points.

Next, a Fourier transform is performed for the time history of each selected node along the chosen lines. This allows the calculation of the spectral content of the motion of the nodes involved. The direct and inverse discrete Fourier transforms are expressed according to the following pair of equations:

$$\begin{aligned}
 v^*[\omega] &= \sum_{t=0}^{N-1} v[t] e^{-i(2\pi/N)\omega t}, & \omega &= 0, 1, \dots, N-1, \\
 v[t] &= \frac{1}{N} \sum_{\omega=0}^{N-1} v^*[\omega] e^{i(2\pi/N)\omega t}, & t &= 0, 1, \dots, N-1,
 \end{aligned}
 \tag{12}$$

where $v[t] = v(t_j)$, $j = 0, \dots, N-1$ is the axial velocity in time, $v^*[\omega] = v^*(\omega_j)$, $j = 0, \dots, N-1$ is the transformed velocity in the frequency domain and $N =$ number of integration

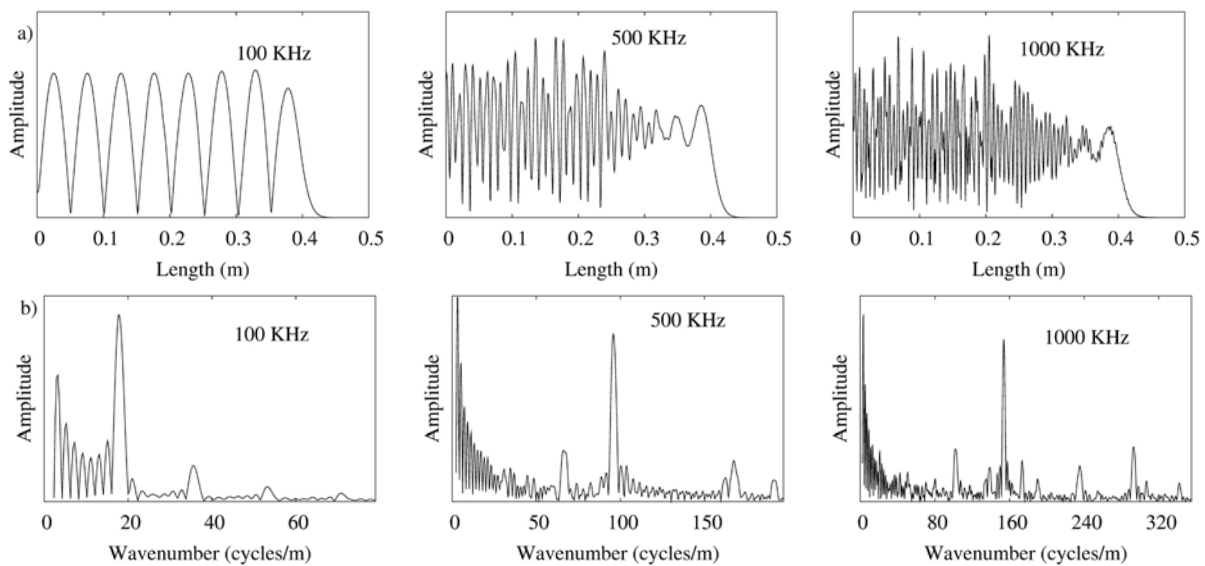


Fig. 5. a) Spatial distribution of axial velocity amplitude over selected nodes parallel to cylinder axis at $3/4$ of the radius, b) the corresponding wavenumber spectrum

steps. The spectrum (amplitude) of v^* can next be computed, and Fig. 4b illustrates, as an example, the frequency content of the time histories of Fig. 4a (ordinates are in logarithmic scale and abscissas in $f = \omega/2\pi$). It is observed that the output signal is broad-band and differs from one point to another. It contains energy at many frequencies and this is useful in order to create the space distribution along the chosen nodes for each frequency.

The last part of the extra step needed for this methodology is to reconstruct the spatial distribution of the response along the pre-defined line(s) (parallel to the axis of the cylinder), for each frequency. From the above frequency spectrum of a node, one can extract the value corresponding to a certain frequency. By repeating the same extraction for all nodes along the line for that frequency, the space distribution is reconstructed. This procedure can be performed for all frequencies of interest included in the frequency spectra.

Fig. 5a shows the reconstruction of the space distribution for three different frequencies along a line parallel to the axis of the cylinder. This figure is similar to Fig. 2a, which refers to the direct methodology with a single harmonic excitation. Although the two figures are not identical, they contain more or less the same information. The last step consists of Fourier transforming the space distribution of the amplitude to get the wavenumber spectrum, as depicted in Fig. 5b, and then the identification of the peaks etc., Eq. (11). A side effect of this methodology is that spurious peaks may sometimes appear on the wavenumber spectrum, which do not belong to the wavenumber value of any of the existing modes, as shown in Fig. 3b. Such peaks can be easily rejected when checked against the analytical solution. These spurious peaks might be a consequence of a possible numerical dispersion as it has been pointed out for the contact-impact problem of a long cylinder by Vales [18] and Gabriel [10]. Of course, the biggest advantage of the step-function load methodology is that it can produce the whole set of the points of the dispersion curves with just one numerical simulation.

4. Numerical results and verification

In this section, some typical numerical results are presented for the two developed methodologies, which have been integrated in the explicit finite element solver code Europlexus [8].

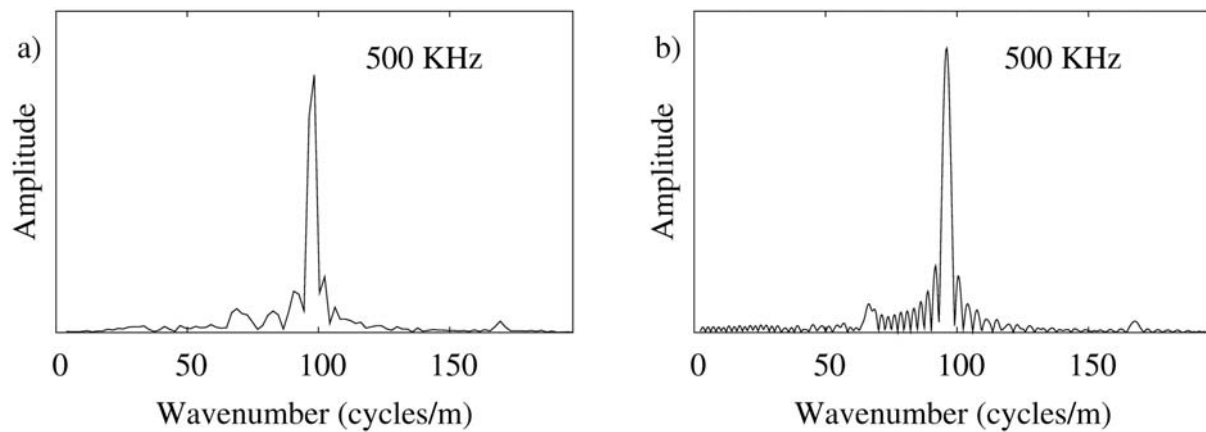


Fig. 6. Wavenumber spectrum: a) without zero padding, b) with zero padding

This code is suitable for fast transient dynamic analysis of fluid-structure systems, and has been jointly developed by the French Commissariat à l’Energie Atomique (CEA Saclay) and the Joint Research Centre of the European Commission (JRC Ispra).

The model used to validate the methodologies is a cylindrical rod with circular cross-section, as described in section 3.2; radius $a = 0.00635$ m and length $L = 0.508$ m, basic finite element model with 32 000 4-node quadrilateral elements (20 elements in the radial direction and 1 600 elements in the axial direction). This model has been selected after some calibration concerning computational time and accuracy. The critical time step for this model is $T_{crit} = 4.25 \times 10^{-8}$ and the selected time step is $T_{selected} = 4 \times 10^{-8}$ which results in a Courant number $N_{Courant} = 0.94$. The same type of mesh, but with 9-node parabolic elements, has also been tested. The accuracy did not improve significantly, while the run-time increased by a factor of 4 (twice because of the extra nodes, and twice because of the decreased time step). Finally, a very coarse model has also been used for quick validation purposes, where the accuracy is acceptable only for very low frequency values.

For the Fast Fourier transformations used for the extraction of the wavenumber spectrum, zero padding has been done at the end of the space distribution, in order to achieve better resolution. By adding zero values in the space distribution (making the model up to 5 times longer), the wavenumber increment Δk can be suitably decreased without altering the spectral content of the signal. With this refinement of the Δk the results are (almost) the same, but the resolution of the curve is much better. Fig. 6 depicts the wavenumber spectrum with and without zero padding and it can be seen that the curve obtained with zero padding is definitely smoother.

Fig. 7a presents the dispersion curves obtained from the numerical simulation with the first 6 modes being included in the plot. The numerical results (points) are compared with the analytical ones (solid curves) and, as can be readily observed, there is very good accuracy. A small perturbation can be noted at the beginning of the numerical curve for the first mode. Apart from that, all other numerical results are very close to the analytical ones. The step function load methodology was used, and, as mentioned previously, the post-treatment was carried out along four lines parallel to the axis of the cylinder (at distances of $1/4$, $2/4$, $3/4$ and $4/4$ radii, correspondingly).

Fig. 7b presents the results (six points) calculated from a simulation with harmonic excitation at the single frequency of 1000 kHz. These results match the corresponding values of the dispersion curves of Fig. 7a for the frequency under consideration. As is evident, at least 60

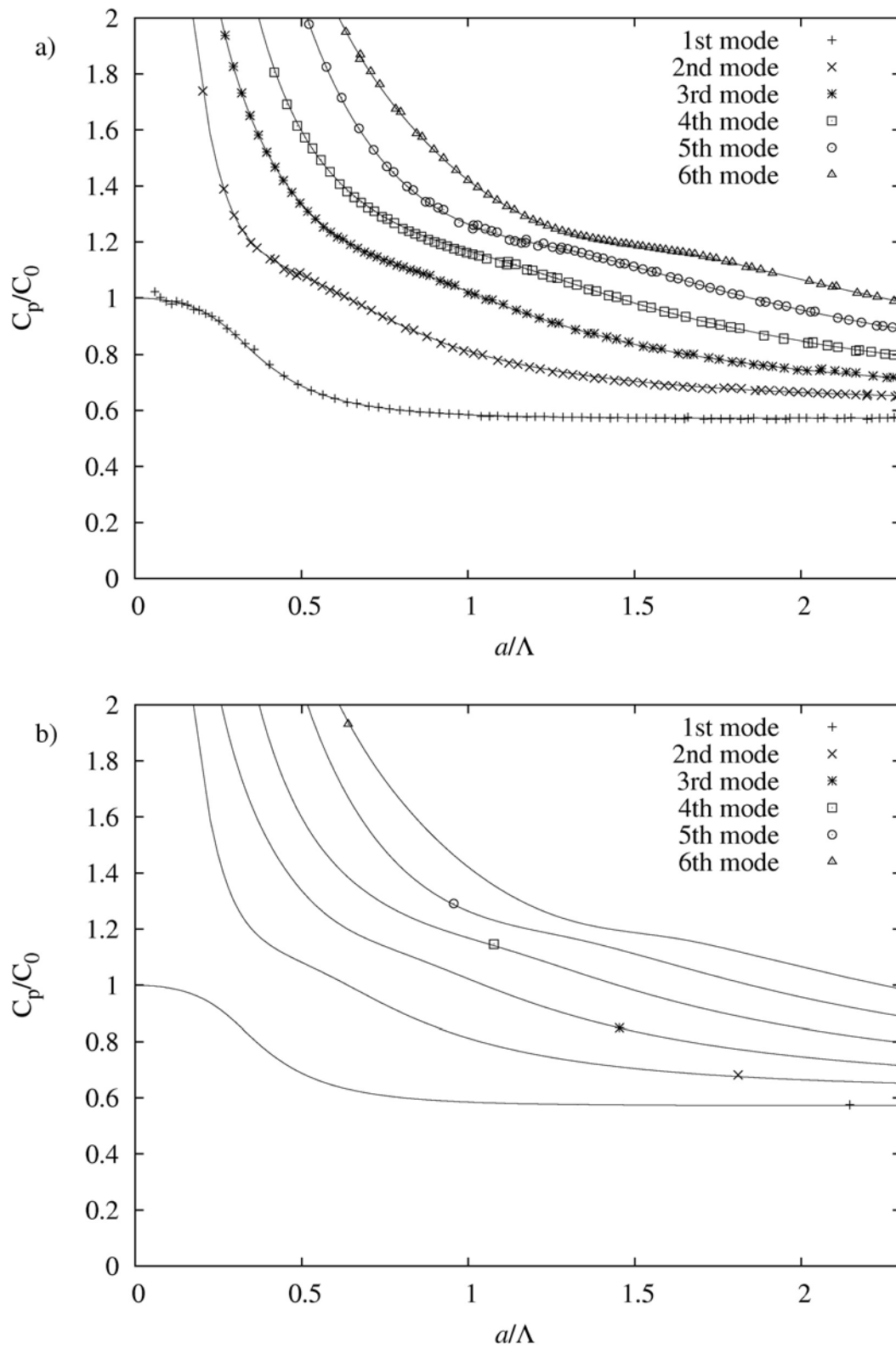


Fig. 7. a) Analytical and numerical dispersion curves with step function load, b) analytical curves and numerical points of dispersion with a single frequency load (1 000 kHz)

simulations would be needed (for 60 points per dispersion curve) in the case of the harmonic load methodology, in order to construct a complete set of dispersion curves. On the contrary, in the case of step function load methodology, just one numerical simulation is sufficient.

By properly selecting parameter values in the model, improvements in the quality of the results can be achieved. For example, it is observed in Fig. 7a that the numerical points of the second mode curve do not include any large ordinate-values, unlike the higher-order mode curves. This is due to the $\Delta\omega$ used in the calculation. In the transformation from the time to the frequency domain, the increment in the frequency is given by $\Delta\omega = 2\pi/T_{end}$ where T_{end} is the final time of the FE calculation. This means that the size of the frequency increment depends (inversely proportional) upon the final time of the simulation, which is limited by the length of the cylinder in order to avoid wave reflections. So, in order to have a better discretization in the frequency domain, a longer model should be used.

Fig. 8a depicts the dispersion curves obtained from a model with a cylinder length of $L = 1.016$ m (twice the length of the standard model). The final time for the simulation is $T_{end} = 18 \times 10^{-5}$ s (twice that of the standard model) and this means that the frequency increment is decreased by a factor of 2 compared to the standard model. It can be observed that in this case the curve of the second mode initiates from larger ordinate-values and also the density of the numerical points on the curves is substantially increased compared to the standard model. This modification of the model gives a more complete set of curves, but the CPU time needed is increased by a factor 4 (2 due to the increase of the model, and 2 due to the increase of the steps needed to reach the final time). Fig. 8b shows the relevant results when second-order elements, 9-node parabolic quadrilaterals, are employed. The slightly better accuracy obtained is at the expense of considerable increase in computation time (time step has been halved and number of nodes doubled), and it would not justify this choice.

As the step function based methodology allows the quick and efficient calculation of the complete set of dispersion curves for a cylindrical rod, it is easy to produce results for several values of the Poisson's ratio. Fig. 9 depicts the dispersion curves for a cylindrical rod with Poisson's ratio: a) $\nu = 0.1$, b) $\nu = 0.49$. The influence of Poisson's ratio on the dispersion curves is evident. For the small Poisson's ratio there is a larger a/Λ -value region where the phase velocity of the first mode is equal to C_0 , while in the case of $\nu = 0.49$, which represents an almost incompressible solid, the phase velocity for the first mode diverges from C_0 even for small values of a/Λ .

Table 1 presents an overview of the models used for the calculation of the results of the current study. The table contains important information concerning the time steps needed for the calculations, the number of the nodes of each model and the total number of time steps. The CPU times needed for the simulations are also included. All calculations were done on a personal computer with an Intel Xeon processor, 2.80 GHz CPU and 2 GB of RAM.

Table 1. Numerical tests

Description	Steps	Nodes	CPU [s]
Coarse mesh with first-order FE	400	1 605	4.08
Fine mesh with first-order FE	2 500	33 621	421.48
Fine mesh with second-order FE	5 000	131 241	1 493.47
Fine mesh with first-order FE, double length	5 000	67 221	1 764.55

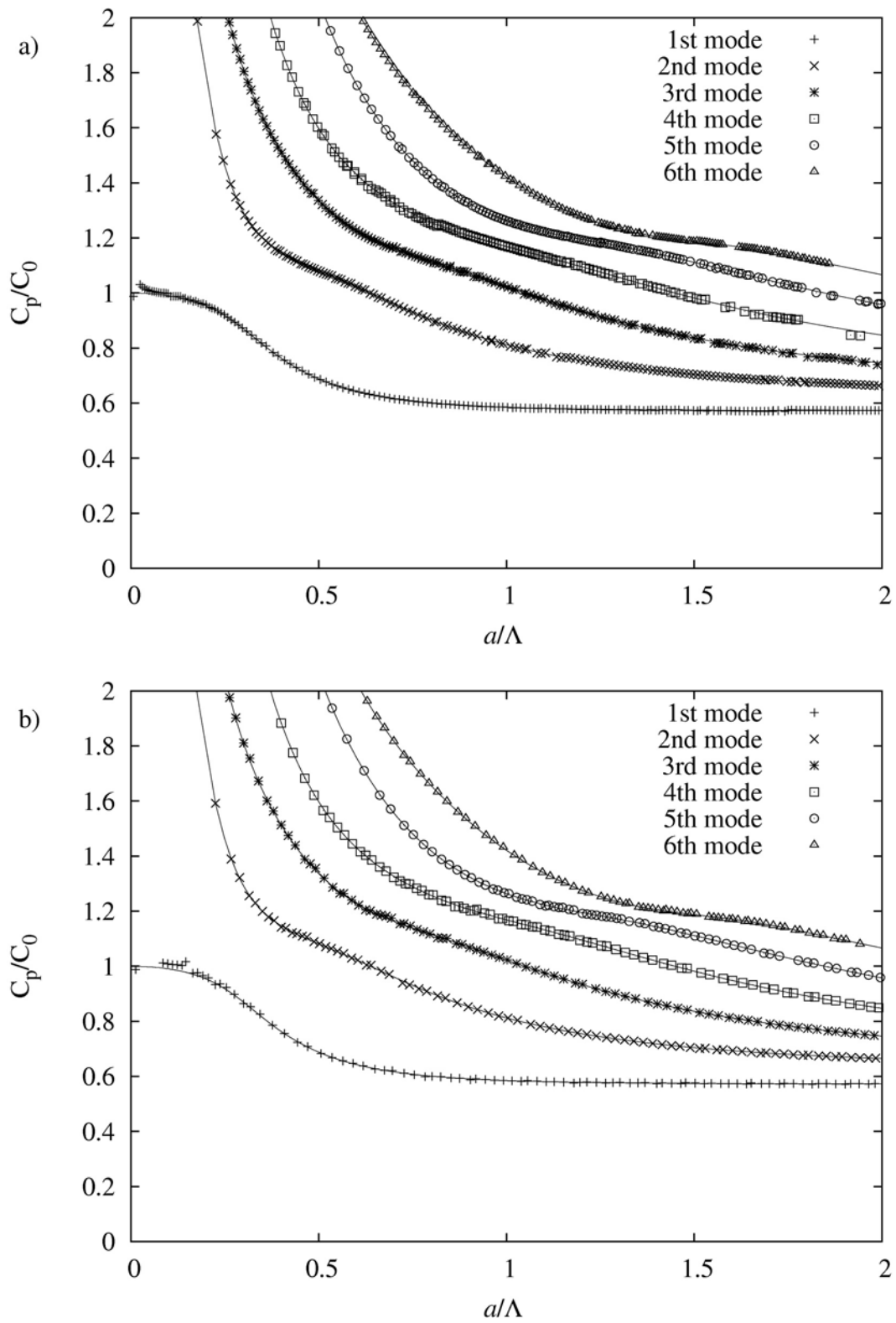


Fig. 8. Analytical and numerical dispersion curve for: a) model with ratio $L/a = 160$, b) model with second-order finite elements

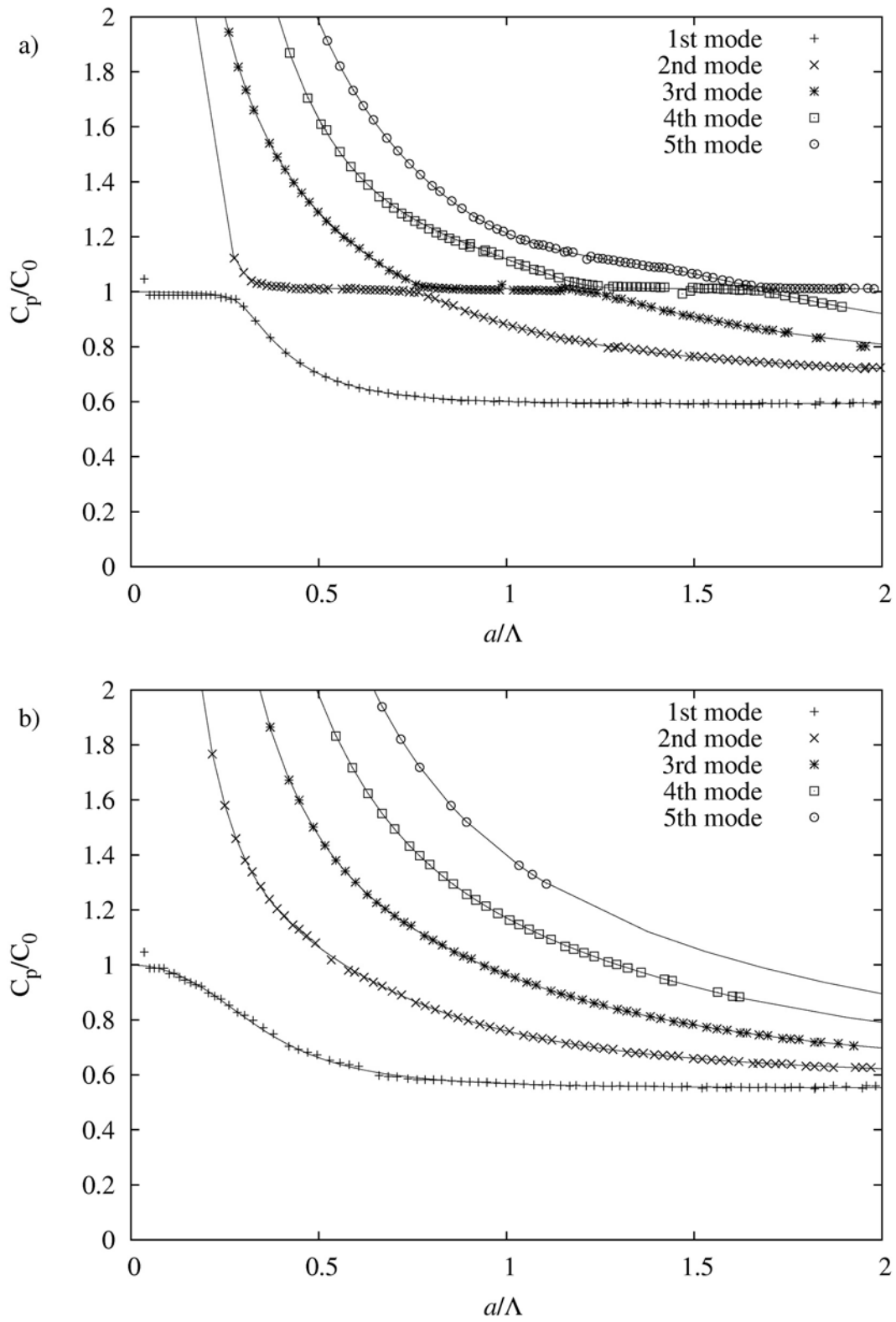


Fig. 9. Analytical and numerical dispersion curves for Poisson's ratio: a) $\nu = 0.1$ and b) $\nu = 0.49$

5. Conclusions

Two alternative methodologies have been presented for determining the dispersion curves of *longitudinal* waves propagating in cylindrical rods with circular cross-section. Both methodologies are based on the post treatment of the results obtained by direct time integration of an explicit finite element model. The numerical solutions were produced by the Europlexus explicit solver, in order to capture the phenomena of wave propagation through the solid. An axisymmetric model has always been used to reduce the CPU time of the calculations.

In the first methodology the excitation on the structure is a single harmonic load and only one specific frequency is triggered. This methodology gives very accurate results, but each FE run determines only one point for each mode dispersion curve. This fact renders this approach inefficient.

In the second methodology the structure is excited with a step function load in order to trigger all the frequencies of the model. This enables the user to produce with the same accuracy all needed outputs with a single run, and this speeds up the total process significantly. Of course a more elaborate post-treatment is required in this case. It has also been observed that in the processing of the response signals some spurious peaks on the wavenumber spectrum may appear, which might be misleading. In practice, however, the appearance of such spurious peaks is not very frequent, so the procedure can be considered quite efficient.

Finally, the accuracy of the two proposed methodologies has been confirmed and illustrated by comparing the dispersion curves produced from the numerical simulations with those of the analytical solution of the Pochhammer-Chree equation. Very close agreement has always been encountered.

References

- [1] Abramowitz, M., Stegun, I. A., Handbook of mathematical functions: With formulas, graphs, and mathematical tables, Dover Publications, 1965.
- [2] Bancroft, D., The velocity of longitudinal waves in cylindrical bars. *Physical Review*, 1941.
- [3] Belytschko, T., Liu, W. K., Moran, B., Nonlinear finite elements for continua and structures, John Wiley & sons, New York, 2000.
- [4] Casadei, F., Halleux, J. P., An algorithm for permanent fluid-structure interaction in explicit transient dynamics, *Computer Methods in Applied Mechanics and Engineering* 128 (1995) 231–289.
- [5] Chree, C., The equation of an isotropic elastic solid in polar and cylindrical coordinates, their solution and applications, *Transactions of the Cambridge Philosophical Society* 14 (1889) 250–369.
- [6] Cooley, J. E., Tukey, J. W., An algorithm for the Machine Calculation of complex Fourier series, *Mathematics of Computation* 19 (2) (1965) 297–301.
- [7] Dennis, J. E., Schnabel, R. B., Numerical methods for unconstrained optimization and nonlinear equations, Prentice-Hall, Englewood Cliffs, 1983.
- [8] EUROPLEXUS user's manual, on-line version: <http://europlexus.jrc.ec.europa.eu>.
- [9] Follansbee, P. S., Frantz, C., Wave propagation in the split Hopkinson pressure bar. *Journal of Engineering Materials and Technology* 105 (1983) 61–66.
- [10] Gabriel, D., Plesek, J., Kolman, R., Vales, F., Dispersion of elastic waves in the contact-impact problem of a long cylinder, *Journal of Computational and Applied Mathematics* 234 (2010) 1930–1936.
- [11] Graff, K. F., Wave motion in elastic solids, Dover publications, New York, 1975.
- [12] Hughes, T. J. R., The finite element method, Dover publications, New York, 1987.
- [13] Kolsky, H., Stress wave in solids, Dover publications, New York, 1963.

- [14] Love, A. E. H., A treatise in the mechanical theory of elasticity, Ph.D. Dover publications, New York, 1944.
- [15] Marais, S. T., Tait, R. B., Cloete, T. J., Nurick, G. N., Material testing at high strain rate using the split Hopkinson pressure bar, *Latin American Journal of Solids and Structures* 1 (2004) 319–339.
- [16] Pochhammer, L., Über die Fortpflanzungsgeschwindigkeiten kleiner Schwingungen in unbegrenzten isotropen Kreiszyylinder (On the propagation velocities of small vibrations in an infinite isotropic cylinder), *Zeitschrift für Reine und Angewandte Mathematik* 81 (1876) 324–336. (in German)
- [17] Puckett, A. D., Fidelity of a finite element model for longitudinal wave propagation in thick cylindrical wave guides, Thesis, Los Alamos national laboratory, New Mexico, 2000.
- [18] Vales, F., Moravka, S., Brepta, R., Cerv, J., Wave propagation in a thick cylinder bar due to longitudinal impact, *JSME International Journal, Series A* 39 (1) (1996) 60–70.
- [19] Redwood, M., *Mechanical waveguides*, Pergamon Press, New York, 1960.
- [20] Zienkiewicz, O. C., *The finite element method*, McGraw-Hill, New York, 1977.